Soldagem & Inspeção

ISSN 1980-6973 (Online) | ISSN 0104-9224 (Print)

TECHNICAL PAPERS

Nitrogen Addition to the Shielding Gas for Welding Hyper-duplex Stainless Steel

André Rocha Pimenta[1], Marilia Garcia Diniz[2], Geronimo Perez[3], Ivan Guillermo Solórzano-Naranjo[4]

[1] Instituto Federal do Rio de Janeiro – IFRJ, Laboratório de Instrumentação e Simulação Computacional Científicas Aplicadas – LISComp, Paracambi, RJ, Brasil.
[2] Universidade do Estado do Rio de Janeiro – UERJ, Programa de Pós-graduação em Engenharia Mecânica, Rio de Janeiro, RJ, Brasil.
[3] Instituto Nacional de Metrologia e Qualidade Industrial – Inmetro, Xerém, RJ, Brasil.
[4] Pontifícia Universidade Católica do Rio de Janeiro – PUC-Rio, Rio de Janeiro, RJ, Brasil.

How to cite: Pimenta AR, Diniz MG, Perez G, Naranjo IGS. Nitrogen addition to the shielding gas for welding hyper-duplex stainless steel. Soldagem & Inspeção. 2019;25:e2512. https://doi.org/10.1590/0104-9224/SI25.12

Abstract: In the present work we have studied the effects of nitrogen addition on the equilibrium of the volume fraction ratio austenite/ferrite and on the structural properties of weldments produced by gas tungsten arc welding (GTAW). The welded joints in tubes UNS S32707 of hyper-duplex steel were produced using argon and nitrogen gas welding, with nitrogen added in ratios of 1.5, 2.5, 3.5, 4.5, and 5.5%. Microstructural characterization of this material under the different processing condition was conducted by means of optical microscopy, scanning electron microscopy, local chemical analysis by X-ray energy dispersive spectroscopy, electron backscatter diffraction Vickers microhardness test, and digital image processing. All welding conditions resulted in welded joints with equiaxial grains microstructure containing austenite both at the boundaries and in the ferrite matrix. Microhardness measurements did not show significant variation in relation to the base metal. The use of welding gases with higher percentages of nitrogen resulted in increases in the austenite volume fraction in the order of 39 to 57% when considering the nitrogen content ranging from 1.5 to 5.5%.

Key-words: Hyper-duplex stainless steel; GTAW; Nitrogen addition; EBSD; Microstructural characterization.

1. Introduction

The family of duplex stainless steels hold this nomination because the microstructure is constituted by balanced volume fractions of ferrite and austenite, resulting in structural materials with good mechanical and corrosion-resistance properties. Such properties ensure them a wide application in the chemical, petroleum and natural gas, and cellulose industries, among others. However, there are still some limitations on the application of this type of steel, such as in seawater in warm environments and in environments subject to extremely aggressive corrosion conditions [1-3]. To meet this demand, a third generation of duplex stainless steels, known as hyper-duplex, has been developed with better corrosion resistance [1]. These steels have chemical compositions with Pitting Resistance Equivalent Number (PREn) around 50, while the previous generation, super duplex stainless steels, have PREn just over 40 [4]. Since hyper duplex steel is recent in the market there are few research reports about this material. Raj et al. [2] and Wang et al. [3] studied the corrosion resistance of hyper-duplex, Raj et al. [2] conclude the pitting resistance was the highest for the sample with more austenite fraction in hot chloride environments, and Wang et al. [3] conclude the precipitation of sigma phase decreased pitting potential of 2707 hyper-duplex. Rajkumar et al. [5] studied the influence of Nb addition and concluded the microstructure of sensitized steel revealed the niobium carbides, resulting in higher hardness and lower erosion rate. Kim et al. [6] studied the influence of Mo, and conclude that the addition of Mo increase the ferrite volume fraction and decreased austenite volume fraction.

When exposed to high energy inputs, such as heat treatments, welding processes, or thermo-mechanical operations, an imbalance in the proportions of ferrite and austenite may occur, as well as the precipitation of deleterious phases, nitrites or carbides, leading to a weakening of the performances of these materials. Fonseca et al. [7] analyzed the formation, kinetics and microstructural evolution of sigma phase in super-duplex UNS S32750, and concluded that sigma phase nucleates on the edges. There is a consensus [7] that the sigma phase precipitates, which nucleates at the austenite/ferrite and ferrite/ferrite interfaces increases the hardness and also causes embrittlement. Kobayashi and Wolnec [8] reported that during sigma phase precipitation in duplex stainless steels, a Cr and Mo-depleted austenitic is formed, thereby explaining the decrease in corrosion resistance. Martins and Casteletti [9] examined the sigma formation in super duplex steel ASTM A890, and the authors concluded that sigma precipitation occurred at a temperature range between 720 °C and 1060 °C, resulting in a drastic decrease in toughness. It is therefore important to further investigate the precipitation of deleterious phase since the presence of those phases may result in components failures, as reported elsewhere [10]. The above-mentioned studies [7-10] were conducted on duplex

Received: 11 Jan.,2020. Accepted: 16 May., 2020.
E-mails: andre.pimenta@ifrj.edu.br (ARP), diniz@uerj.br (MGD), perezgeronimo@hotmail.com (GP), guilsol@puc-rio.br (IGSN)

This is an Open Access article distributed under the terms of the Creative Commons Attribution Non-Commercial License which permits unrestricted non-commercial use, distribution, and reproduction in any medium provided the original work is properly cited.

(first generation) or super duplex (second generation). In a second study [11] the authors have worked on hyper duplex (third generation) steels and found that the precipitation kinetics of sigma phase is faster than in the other 2 generations steels, due to a higher percent of chromium and molybdenum.

The weldability of steels is always an important factor to be evaluated since it is the most common and often the only technique possible to be used for joining components. Welding processes usually involve sufficient heat input to cause microstructural changes in steels which are rich in alloying elements. Kim et al. [12] performed GTAW welding tests with Ar shielding gas in a hyper-duplex steel getting equal volume fractions of ferrite and austenite for welding with a filler metal, however the joint without a filler metal, presented 80% of ferrite, thus exhibiting a low corrosion resistance. In a more recent study [13], the authors have investigated the possibility to improve the weld joint without filler metal by the addition of 2% N_2 in the shielding gas. With the addition of N_2, Kim et al. [13] reached a welded joint with 60% of ferrite, still a higher value than the ideal volume fraction of 50% ferrite.

It is well known that nitrogen is a strong austenite stabilizer [13-15]. However, there are no studies reported in the literature determining the optimum percentage of N_2 that should be added in the shielding gas to promote equal volume fractions of ferrite and austenite, especially on hyper-duplex stainless steel. In this context, the present work aims at determining the amount of N_2 that should be added to the shielding gas for manufacturing an autogenous GTAW joint in hyper-duplex steel.

2. Materials and Methods

The material used for this work was hyper-duplex tubes with 19.05 mm in diameter and 2.24 mm in thickness. Those tubes were welded in our laboratory in an automated manner using the gas tungsten arc welding (GTAW) process, using a heat input of 0.15 kJ/mm and a shielding gas composed of Ar + N_2 with different contents of commercially standard N_2, 1.5%, 2.5% (commercial standard), 3.5%, 4.5% and 5.5%. The standard chemical composition expected for UNS S32707 steel and our results obtained from a quantitative chemical analysis by optical emission are shown in Table 1. The welding heat input calculation was performed by using the Equation 1 [16].

$$H = \eta E I / 1000 S \quad (1)$$

Where, “H” is the heat input (0.15 kJ/mm), “η” is the arc efficiency (0.8 [17]), “E” is the arc voltage (10 V), “I” is the arc current (32 A) and “S” is the travel speed (1.70 mm/s).

Table 1. Expected chemical composition and results obtained by optical emission for the material used (wt%).

Element	Standard	Optical emission
C	max. 0.030	0.035
Si	max. 0.5	0.258
Mn	max. 1.5	0.84
P	max. 0.035	0.010
S	max. 0.010	0.0059
Cr	27	25.81
Ni	6.5	6.40
Mo	4.8	4.77
N	0.4	---------
Co	1.0	1.07

The following welding parameters were used: pulsed arc; peak current intensity of 40 A; base current intensity of 24 A; peak and base current time 50%; shielding gas flowrate of 13 L/min; AWS Class EWTH-2 2.4 mm electrode; electrode tip angle of 37 °; and welding nozzle #5.

In order to analyze the microstructures of the weld metal (WM), the heat affected zone (HAZ) and the base metal (BM), we have used light optical microscopy (LOM) and scanning electron microscopy (SEM) equipped with X-ray energy dispersive spectroscopy (EDS). The LOM images were taken on a Zeiss M2m microscope, and the SEM images were documented on a FEI Nova Nanolab 600 FEG-SEM microscope operating at 10 kV. For LOM observations the samples were polished with diamond paste and submitted to electrolytic etching with NaOH solution. For the SEM observation, the samples fist were polished with diamond paste and finally electrochemical polishing with a chromium oxide solution.

FEG-SEM allowed phase identification through electron backscatter diffraction (EBSD) and chemical mapping by means of energy dispersive spectrometry - EDS. Both EBSD and EDS analyses were carried out on welded joints with 2.5% N_2, which is the commercial standard for shielding gas, and 5.5% N_2, which corresponds to the highest nitrogen content in our tests. In fact, the literature [18,19] reports that 5.5% N2 should be the situation with the highest propensity to form nitrites.

The volume fractions of ferrite and austenite present in the base metal (BM), heat affected zone (HAZ) and welded metal (WM) of the welded joint were quantified by digital image processing using Zeiss AxioVision software. Vickers microhardness (HV) were measured on the welded joints following a straight line, covering the WM, HAZ and BM of the joint in distance intervals of 100 µm as illustrated in Figure 1. A PANTEC microhardness indenter model MV-1000A, with a 0.9807 N force and load application time of 15 seconds was used.

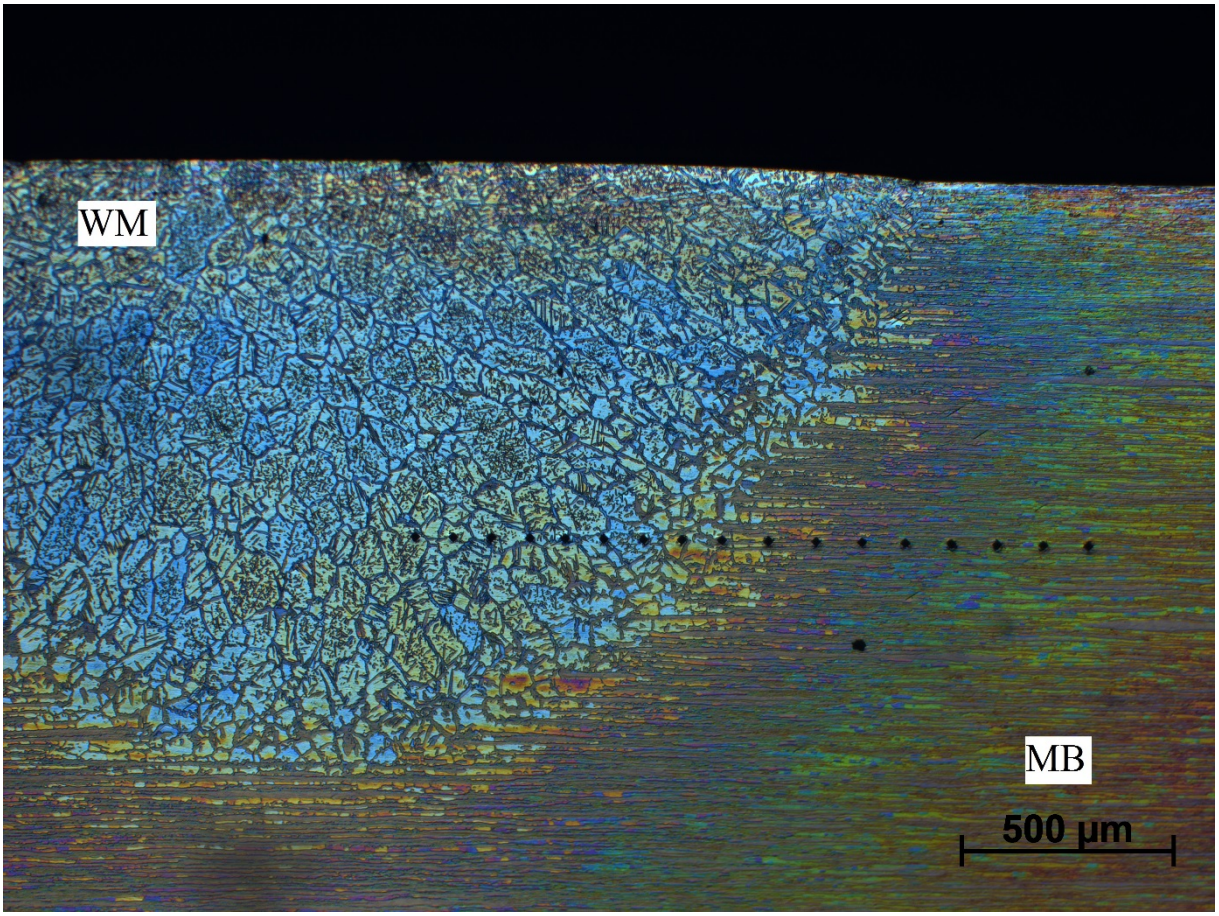

Figure 1. Optical micrograph of a welded joint showing the 3 zones in a welded joint and the position marks where Vickers microhardness were measured.

3. Results and Discussion

Figure 2 shows a set of optical micrographs representative of the five nitrogen concentrations used in the welding at different magnifications and sample regions. The electrolytic etchant, which deposits a layer of oxides on the surface of the sample [20], allows color effects under reflection LOM, revealing the ferrite phase in yellow, blue and red colors and austenite in shades of brown to slightly bluish. None of the welded joints showed the presence of a sigma phase, which would have appeared with a dark brown color and a lacy aspect [21].

In the WM micrographs shown in Figure 2 it is possible to observe that in all the conditions studied here, the grains appears preferentially equiaxed. The pulsed arc process used in welding leads to the stirring of the weld pool, resulting in a better distribution of heat flowing during the solidification process, supporting the nucleation of growth of equiaxed grains [22].

The BM presented a microstructure with alternating ferrite and austenite lamellae (Welding Zone 200x - Figure 2). Such alternation is associated with the ferrite/austenite interfacial energy being lower than that for ferrite/ferrite and austenite/austenite boundaries. The size of the BM grains of the studied hyper-duplex steel is small when compared to those in the duplex and super-duplex steels of the same manufacturer. The obtained images indicate that the width of the ferrite and austenite grains was less than 10 µm, a fact that may explain the high mechanical strength of the hyper-duplex steels when compared to the previous generation steels [4].

The HAZs appears to be rather narrow, measuring less than 0.1 mm (HAZ 1000x - Figure 2). This is in accordance with the welding process used because the heat input in GTAW welds is very localized [23]. The presence of deleterious (sigma) phases was not observed in the HAZs (Figure 2).

In the regions of the WMs (WM 1000x - Figure 2) it was verified that the austenite was formed preferentially in ferrite grain boundaries, with same nucleation inside the ferrite grain. In the solidification of the duplex steels, the ferrite phase is usually formed first, and the austenite precipitates from it when the material is already in the solid state [24]. Qualitatively, it is possible to observe a direct relationship between the increase in the amount of nitrogen in the shielding gas and the increase of the volume fraction of austenite in the WM, which is due to the strong austenitizing effect of nitrogen [25]. It is also possible to notice the presence of allotriomorphic austenite, which is found in ferrite grain boundaries [26].

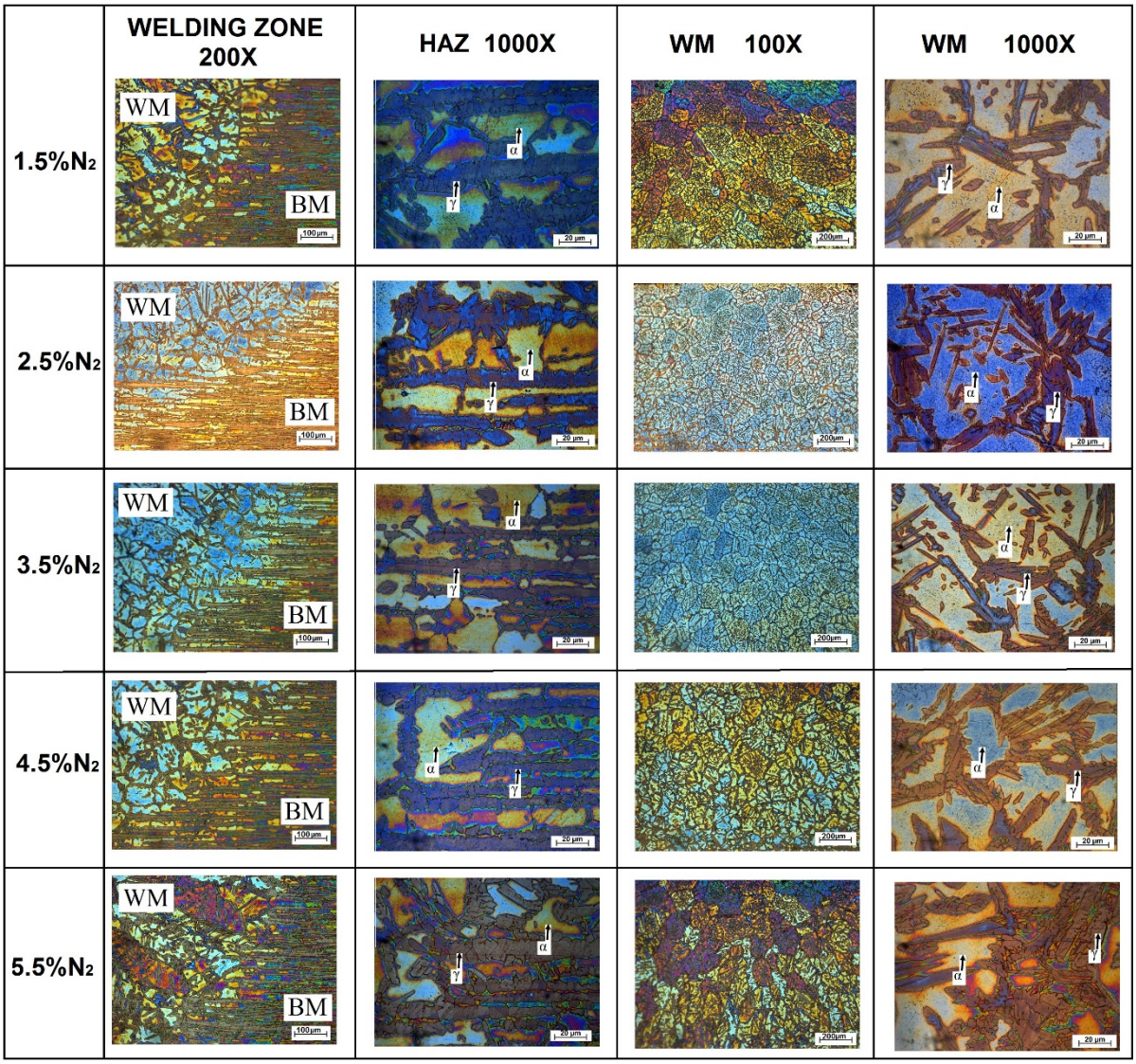

Figure 2. OM images of the weld joints for all conditions showing the BM, HAZ and WM. Austenite in brown color; and Ferrite in yellow, blue and red colors

Some microstructural features observed by SEM under 20,000 magnification (Figure 3) identified small regions within the ferrite and austenite grains. Dark-colored regions with the same geometric aspect had already been identified by other investigators as nitrides [18,19]. However, local EDS results indicated no composition changes that could be associated with the presence of deleterious phases (Figure 3), which according to the literature [18], would be regions richer in chromium, molybdenum, or nitrogen. According ASM standards [23] the formation of nitrides and deleterious phases requires the duplex stainless steel to be held at high temperature for a given time. However, due to the fact the autogenous process has a very high cooling rate, the welding process allowed no time for nitrides or deleterious phases formation.

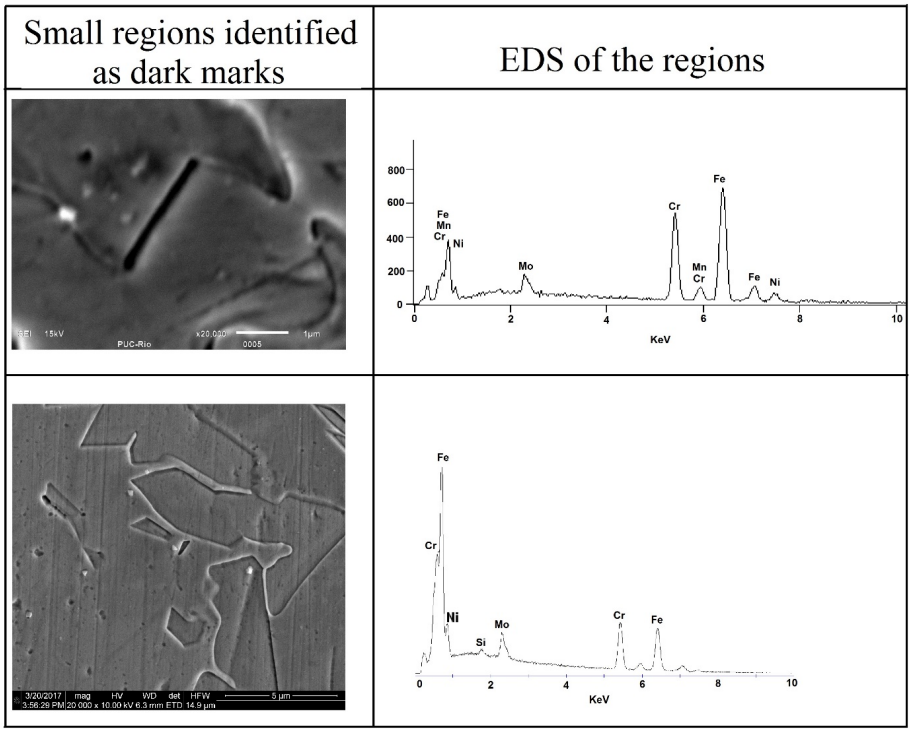

Figure 3. SEM images and EDS spectrum of regions within the ferrite and austenite grains.

Due to the deleterious effect of the sigma and chi phase, nitrites and carbides, we explored the capabilities of three techniques to verify their formations: secondary electrons SEM, EBSD and microhardness. The EBSD results (Figure 4) indicate only the presence of ferrite and austenite phases (alpha phase in red and gamma phase in green). As expected the EDS maps (Figure 5) for the Ni, Cr, Mo and N elements show that the austenite had higher levels of Ni and N and the ferrite had higher levels of Mo [27]. Cr was homogeneously-distributed in both phases.

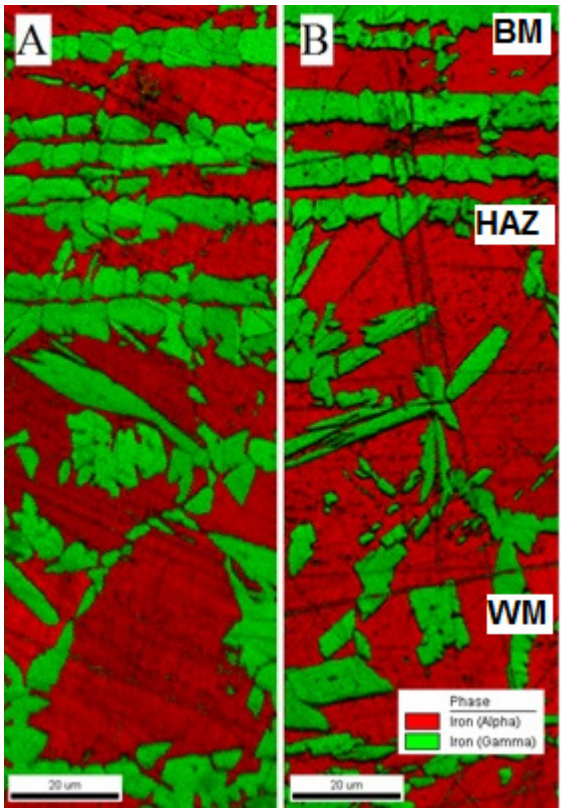

Figure 4. EBSD results of a welded joints with 2.5% N_2 (A) and 5.5%N_2 (B) showing the BM, HAZ and WM.

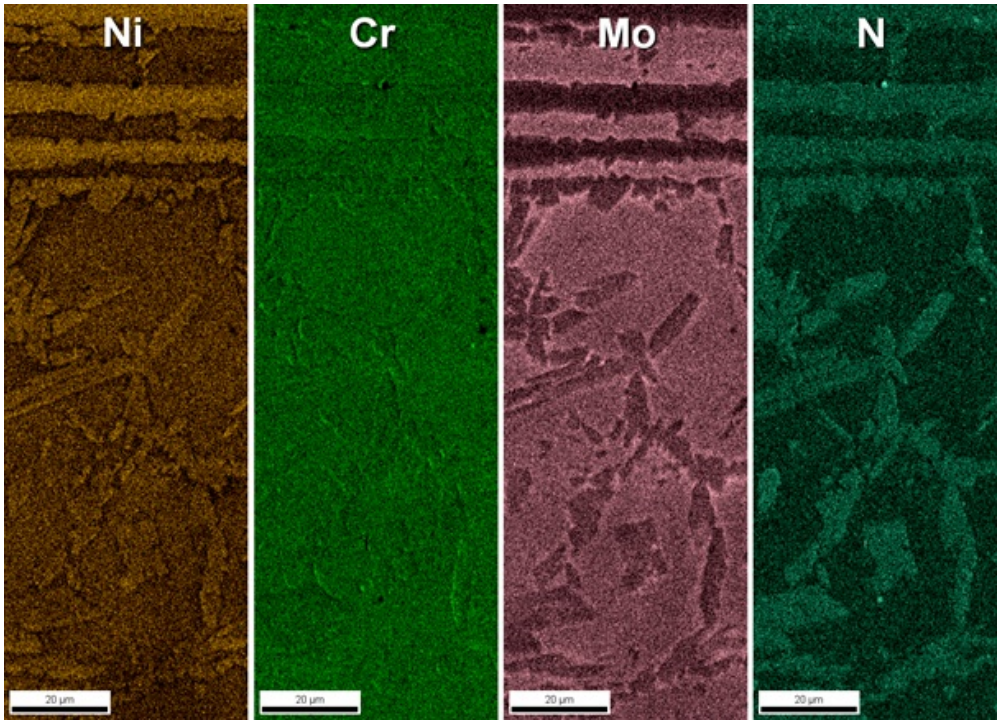

Figure 5. X-ray elemental maps of welded joint.

The increase of the nitrogen content used in the shielding gas had no significant effect in the microhardness of the welded joints, as shown in Figure 6. A statistical analysis using Student's t-test, with 95% confidence, showed that there was no variation between the BM and WM regions. The homogeneity in the microhardness values is another indicator of the absence of any deleterious second phase precipitation [12].

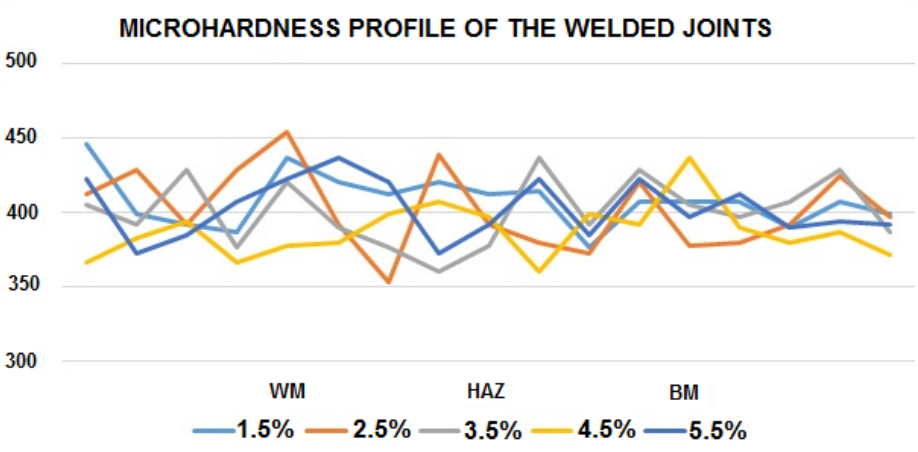

Figure 6. Microhardness profiles of welded joints following a straight line covering the WM, HAZ and BM.

The plot in Figure 7 shows the austenite volume fractions obtained for each of the welded joints conditions and the BM. It is possible to establish a direct relationship between the increase in the nitrogen content in the shielding gas and the increase in the austenite volume fraction in the WMs. The duplex structure stainless steel has an ideal volume fraction ratio around 50% for each of the phases, ferrite and austenite [28]. The literature indicates acceptable ranges for the volume fractions variations of each phase, which could range between 30% and 70% [29] or between 35% and 65% [30], values valid for both phases, ferrite and austenite. For the indicated limits, all conditions used in this study have presented satisfactory results, with volume fraction values of austenite ranging from 39% to 57%. An important finding in the present work is that for the shielding gas with nitrogen between 3.5% and 4.5%, the measured volume fractions were the only ones that reached closely the ideal value of 50%.

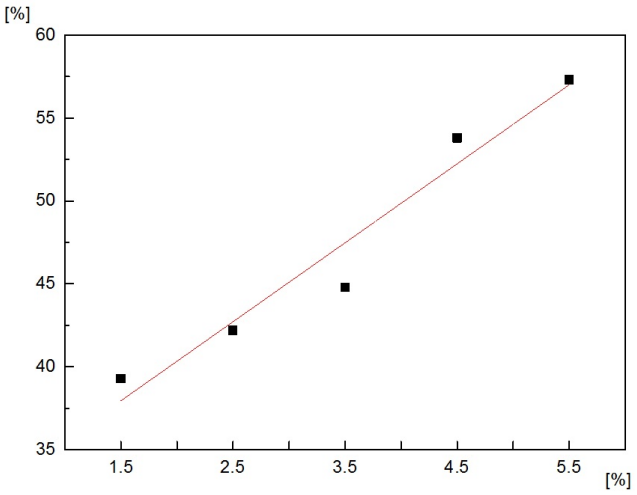

Figure 7. Effects of the variation of the N_2 content in the shielding gas on the volumetric fraction of the austenite phase.

4. Conclusions

Consistent observations of the microstructure of weld joints in hyper-duplex stainless steel upon shielding gas composed of Ar + N2 with different contents of N_2 yield to following conclusions:

- It is marked the effect of the amount of nitrogen on the austenite volume fraction: It is possible to observe an almost linear relationship between the increase in the amount of nitrogen and the volume fraction of austenite in weld metal. Using the commercial standard shielding gas, with 2.5% of N_2, the WM has 42% of austenite. For contents between 3.5% and 4.5% the ideal volume fraction of austenite was found as 50%, indicating a need for review of currently used industrial processes;
- The three techniques explored to verify the formations of sigma and chi phases, nitrites and carbides did not indicate their formation. The microhardness indicated no change between WM, HAZ and BM. The EDS SEM and EBSD analyses only indicated the presence of phases ferrite and austenite. It is very important to prove that the increase in the amount of N_2 required to achieve a 50% volumetric fraction of austenite did not result in deleterious phases formation.

References

[1] Stenvall P, Holmquist M. Weld properties of sandvik SAF 2707 HD. La Metallurgia Italiana. 2008;10:11-18.

[2] Raj PN, Sivan AP, Sekar K, Joseph MA. Effect of austenite reformation on localized corrosion resistance of hyper-duplex stainless steel in hot chloride solution. International Journal of Metalcasting. 2019;14(1):167-178.

[3] Wang J, Chen W, Meng H, Cui Y, Zhang C, Han P. Influence of sigma phase on corrosion and mechanical properties of 2707 hyper-duplex stainless steel aged for short periods. Journal of Iron and Steel Research International. 2019;26(5):452-461. http://dx.doi.org/10.1007/s42243-018-0175-3.

[4] Chai G, Kivisakk U, Tokaruk J, Eidhagen J. Hyper duplex stainless steel for deep subsea applications. Stainless Steel World. 2009;27:1-5.

[5] Rajkumar M, Kumaresh Babu SP, Vallimanalan A, Mahendran R. Room-Temperature Erosion Behaviour of Nb-Stabilized 27Cr–7Ni–Mo–W–N Cast Hyper-Duplex Stainless Steel (Nb + CD3MWN - 7A). Journal of the Instituition of Engineers (India). 2019;100(1):83-90. http://dx.doi.org/10.1007/s40033-018-0171-6.

[6] Kim N, Gil W, Lim H, Choi C, Lee H. Variation of mechanical properties and corrosion properties with Mo contents of hyper duplex stainless-steel welds. Metals and Materials International. 2019;25(1):193-206. http://dx.doi.org/10.1007/s12540-018-0166-8.

[7] Fonseca GS, Oliveira PM, Diniz MG, Bubnoff DV, Castro JA. Sigma phase in superduplex stainless steel: formation kinetics and microstructural path. Materials Research. 2017;20(1):249-255. http://dx.doi.org/10.1590/1980-5373-mr-2016-0436.

[8] Kobayashi DY, Wolynec S. Evaluation of the low corrosion resistant phase formed during the sigma phase precipitation in duplex stainless steels. Materials Research. 1999;2(4):239-247. http://dx.doi.org/10.1590/S1516-14391999000400002.

[9] Martins M, Casteletti LC. Sigma phase morphologies in cast and aged super duplex stainless steel. Materials Characterization. 2009;60(8):792-795. http://dx.doi.org/10.1016/j.matchar.2009.01.005.

[10] Tavares SSM, Pardal JM, Almeida BB, Mendes MT, Freire JLF, Vidal AC. Failure of superduplex stainless steel flange due to inadequate microstructure and fabrication process. Engineering Failure Analysis. 2018;84:1-10. http://dx.doi.org/10.1016/j.engfailanal.2017.10.007.

[11] Zhang B, Jiang Z, Li H, Zhang S, Feng H, Li H. Precipitation behavior and phase transformation of hyper duplex stainless steel UNS S32707 at nose temperature. Materials Characterization. 2017;129:31-39. http://dx.doi.org/10.1016/j.matchar.2017.04.018.

[12] Kim JS, Kim ST, Lee IS, Jang SH, Park YS, Kim KT, et al. Mechanism of localized corrosion and phase transformation of tube-to-tube sheet welds of hyper duplex stainless steel in acidified chloride environments. Materials Transactions. 2012;53(12):2166-2174. http://dx.doi.org/10.2320/matertrans.M2012243.

[13] Kim HJ, Jeon SH, Kim ST, Park YS. Influence of the shielding gas composition on the passive film and erosion corrosion of tube-to-tube sheet welds of hyper duplex stainless steel. Corrosion Science. 2015;91:140-150. http://dx.doi.org/10.1016/j.corsci.2014.11.014.

[14] Kim ST, Lee IS, Kim JS, Jang SH, Park YS, Kim KT, et al. Investigation of the localized corrosion associated with phase transformation of tube-to-tube sheet welds of hyper duplex stainless steel in acidified chloride environments. Corrosion Science. 2012;64:164-173. http://dx.doi.org/10.1016/j.corsci.2012.07.014.

[15] Kim HJ, Jeon SH, Kim ST, Lee IS, Park YS, Kim KT, et al. Investigation of the sensitization and intergranular corrosion of tube-to-tubesheet welds of hyper duplex stainless steel using an electrochemical reactivation method. Corrosion Science. 2014;87:60-70. http://dx.doi.org/10.1016/j.corsci.2014.06.005.

[16] ASM International . ASM handbook. Vol. 9: metallography and microstructure. Ohio: ASM International; 1989.

[17] Fuerschbach PW, Knorovsky GA. A study of melting efficiency in plasma arc and gas tungsten arc welding. Welding Journal. 1991;70:287-297.

[18] Jeon S-H, Kim S-T, Kim J-S, Kim J-S, Kim K-T, Park Y-S. Effects of copper addition on the precipitation of chromium nitrides and the associated pitting corrosion resistance of the hyper duplex stainless steels. Materials Transactions. 2012;53(12):2129-2134. http://dx.doi.org/10.2320/matertrans.M2012277.

[19] Jang SH, Kim ST, Lee IS, Park YS. Effect of shielding gas composition on phase transformation and mechanism of pitting corrosion of hyper duplex stainless steel welds. Materials Transactions. 2011;52(6):1228-1236. http://dx.doi.org/10.2320/matertrans.M2010414.

[20] Elmer JW, Palmer TA, Specht ED. Direct observations of sigma phase formation in duplex stainless steels using in-situ synchrotron x-ray diffraction. Metallurgical and Materials Transactions. A, Physical Metallurgy and Materials Science. 2007;38(3):464-475. http://dx.doi.org/10.1007/s11661-006-9076-3.

[21] Magnabosco R. Kinetics of sigma phase formation in a duplex stainless steel. Materials Research. 2009;12(3):321-327. http://dx.doi.org/10.1590/S1516-14392009000300012.

[22] Wang SH, Chiu PK, Yang JR, Fang J. Gamma phase transformation in pulsed GTAW weld metal of duplex stainless steel. Materials Science and Engineering A. 2006;420(1-2):26-33. http://dx.doi.org/10.1016/j.msea.2006.01.028.

[23] ASM International. ASM handbook. Vol. 6: welding brazing and soldering. Ohio: ASM International; 1993.

[24] Padilha AF, Plaut RL. Phase transformation and microstructure. In: Alvares A, Degallaix M, editors. Duplex stainless steels. Hoboken: John Wiley & Sons; 2009. p. 115-139.

[25] American Society for Testing and Materials. ASTM:A800/A 800M - 01 Standard pratice for steel casting, austenitic alloy, estimating ferrite content thereof, ferrous casting, ferroalloys. West Conshohocken: ASTM; 2001.

[26] Fonseca GS, Barbosa LOR, Ferreira EA, Xavier CR, Castro JÁ. Microstructural, mechanical, and electrochemical analysis of duplex and superduplex stainless steels welded with the autogenous TIG process using different heat input. Metals. 2017;7(12):538558. http://dx.doi.org/10.3390/met7120538.

[27] Hammar O, Svensson U. Solidi cation and casting of metals. London: The Metals Society; 1979.

[28] Nilsson JO. Super duplex stainless steels. Materials Science and Technology. 1992;8(8):685-700. http://dx.doi.org/10.1179/mst.1992.8.8.685.

[29] Urena A, Otero E, Utrilla MV, Munez CJ. Weldability of a 2205 duplex stainless steel using plasma arc welding. Journal of Materials Processing Technology. 2007;182(1-3):624-631. http://dx.doi.org/10.1016/j.jmatprotec.2006.08.030.

[30] Menezes JWA, Reis FEU, Abreu HFG, Miranda HC, Ribeiro JEM, Oliveira HR. Efeito da energia de soldagem sobre a fração volumétrica da fase ferrítica no aço inoxidável duplex UNS S31803. In: Anais do III Congresso Brasileiro de P&D em Petróleo e Gás; 2005; Salvador. Natal: Associação Brasileira de P&D em Petróleo e Gás; 2005. p. 1-6.